LETTERS

Serial time-encoded amplified imaging for real-time observation of fast dynamic phenomena

K. Goda[1]*, K. K. Tsia[1]* & B. Jalali[1]*

Ultrafast real-time optical imaging is an indispensable tool for studying dynamical events such as shock waves[1,2], chemical dynamics in living cells[3,4], neural activity[5,6], laser surgery[7–9] and microfluidics[10,11]. However, conventional CCDs (charge-coupled devices) and their complementary metal–oxide–semiconductor (CMOS) counterparts are incapable of capturing fast dynamical processes with high sensitivity and resolution. This is due in part to a technological limitation—it takes time to read out the data from sensor arrays. Also, there is the fundamental compromise between sensitivity and frame rate; at high frame rates, fewer photons are collected during each frame—a problem that affects nearly all optical imaging systems. Here we report an imaging method that overcomes these limitations and offers frame rates that are at least 1,000 times faster than those of conventional CCDs. Our technique maps a two-dimensional (2D) image into a serial time-domain data stream and simultaneously amplifies the image in the optical domain. We capture an entire 2D image using a single-pixel photodetector and achieve a net image amplification of 25 dB (a factor of 316). This overcomes the compromise between sensitivity and frame rate without resorting to cooling and high-intensity illumination. As a proof of concept, we perform continuous real-time imaging at a frame speed of 163 ns (a frame rate of 6.1 MHz) and a shutter speed of 440 ps. We also demonstrate real-time imaging of microfluidic flow and phase-explosion effects that occur during laser ablation.

Optical imaging is a widespread and versatile diagnostics and inspection tool in use today. Although most of the current research in imaging is aimed at improving the spatial resolution to below the diffraction limit[12,13], there are numerous applications that demand improvement in temporal resolution. Imaging systems with high temporal resolution are needed to study rapid physical phenomena ranging from shock waves, including extracorporeal shock waves used for surgery[1], to diagnostics of laser fusion[2] and fuel injection in internal combustion engines. High-speed imaging is becoming increasingly important in microscopy because on the micrometre scale even slow-moving phenomena require high temporal resolution. One example is the spatiotemporal study of biochemical waves in cells and tissues, which requires imaging with a micro- to nanosecond response time and is important for the study of cell signalling and drug transport[14]. Another key application is in the field of flow cytometry[11], where high-speed cameras are needed to provide high-throughput cell characterization.

The CCD or CMOS imager is by far the most widely deployed optical imaging technology. It offers a spatial resolution of a few micrometres, a large number of pixels and relatively low cost. Typical imagers used in consumer electronics have frame rates of 30 Hz, although high-end versions can operate at rates on the order of 1 kHz by reducing the number of pixels that are read out from the arrays. A CCD imager with a 1-MHz frame rate—the world's fastest CCD camera—has been developed by Shimadzu Corporation (ref. 15; see also http://www.shimadzu.com/products/test/hsvc/oh80jt0000001d6t-att/booe13-02.pdf). Its impressive performance stems from several technological modifications aimed at overcoming the loss of sensitivity that results from the shorter integration time during high-speed imaging, and also at reducing the time it takes to read out the data from the 2D pixel arrays. These modifications include a larger pixel size for the purpose of adding pixel-level *in situ* memory (at the expense of reduced spatial resolution), and cooling of the camera to reduce noise (at the expense of the added complexity of refrigeration). The Shimadzu device also relies on a high-power illuminator to ensure adequate signal-to-noise ratio and to prevent a drop in sensitivity—a requirement that renders it unsuitable for microscopy, where focusing of the high-power illumination over a small field of view can cause damage to a biological sample. This compromise between sensitivity and frame rate is not unique to the CCD—it impacts almost all imaging and detection systems.

In scientific applications, high-speed imaging is often achieved using the time-resolved pump–probe technique[16–18]. Pump–probe techniques can capture the dynamics of fast events, but only if the event is repetitive. Because they do not operate in real time, they are unable to capture non-repetitive random events that occur only once or do not occur at regular intervals, such as rogue events[19]. Detection of such events requires an imaging technology with fast, continuous, real-time capability.

Another type of high-speed image sensor is the framing streak camera, which has been used for diagnostics in laser fusion, plasma radiation and combustion. This device operates in burst mode only (providing only several frames; see http://learn.hamamatsu.com/tutorials/streakcamera/) and requires synchronization of the camera with the event to be captured, rendering streak cameras also unable to capture unique or random events. This, along with the high cost of the camera, limits its use in practical applications.

Although CCD imagers will continue to be the most widely used imaging modality and pump–probe experiments will remain a powerful tool for studying fast repetitive events, a new and complementary imaging modality that can capture the dynamics of fast single-shot or random events is clearly needed. Serial time-encoded amplified microscopy (STEAM) technology is a new approach to imaging that provides such a capability. The 2D image is encoded into a serial time-domain waveform that is amplified and captured, not by a CCD camera, but instead by a single-pixel photodiode and an oscilloscope. The main attributes of the new imager are the image amplification in the optical domain and the elimination of the CCD—when combined, they enable continuous real-time operation at a frame rate of 6.1 MHz and a shutter speed of 440 ps. The STEAM camera operates continuously and can capture ultrafast events

[1]Department of Electrical Engineering, University of California, Los Angeles, California 90095, USA.
*These authors contributed equally to this work.

without any knowledge of the timing of their occurrence. The throughput of the STEAM camera can be further increased with minor modifications to the system shown in Fig. 1 (see Methods and Supplementary Information.)

The key feature of the STEAM camera is the mapping of a 2D image into an amplified serial time-domain waveform. This is achieved by first encoding the 2D spatial information of an object onto the spectrum of a broadband (continuum) pulse (Fig. 1) using a pair of orthogonally oriented spatial dispersers (Methods). A similar component has previously been used for spectroscopy[20]. The encoding occurs when the spatially dispersed pulse is reflected off the object, after which it re-enters the disperser, where the wavelengths are recombined. An optical circulator directs the pulses into an optically amplified dispersive Fourier transformer, the details of which are shown in the inset of Fig. 1.

Image amplification is performed in the optical domain and occurs in two stages. An erbium-doped fibre amplifier pre-amplifies the image by 10 dB (a factor of ten). The image then enters a dispersive fibre whose function is twofold. By virtue of high group-velocity dispersion (also called temporal dispersion), the dispersive fibre performs a Fourier transform operation, mapping the spectrum into the time domain. The optical spectrum, which is encoded with the spatial image, now appears as a serial sequence in time (Fig. 2a). To amplify the image simultaneously (second-stage amplification), the dispersive fibre is pumped with secondary light sources to implement stimulated Raman amplification directly within the dispersive medium. This technique is crucial because it not only compensates for the loss inherent in the dispersive fibre, but also provides an additional net image amplification of 15 dB (a factor of 31.6). Therefore, the system amplifies the image by a total of 25 dB (a factor of 316) in the optical domain.

Dispersion-compensating fibre (DCF) is used to perform the dispersive Fourier transform and Raman amplification of the image because it offers high dispersion and low loss as well as a high Raman gain coefficient[21–23]. Broadband gain can be achieved by pumping with multiple lasers or an incoherent light source[22]. As the image enters the DCF, the aperture of the fibre rejects the scattered light from out-of-focus planes, rendering the system a confocal microscope.

The amplified dispersive Fourier transform maps the spectrum of an optical pulse into a time-domain waveform, allowing the spectrum to be viewed on a conventional electronic receiver (Fig. 2a). It eliminates the traditional spectrometer, including the prism or diffraction grating and the CCD, and makes it possible to capture the spectrum with a single-pixel photodetector. At the same time, it overcomes the receiver noise level by amplifying the signal while it is still in the optical domain. Optical image amplification is vital for high-speed imaging because the noise power present in any measurement increases inversely with the integration time. Without this amplification, the image would not be visible because the signal would lie below the thermal noise level of the photodetector, as can be seen in Fig. 2b. A high-power laser source can also overcome the detector noise; however, this is not a desirable solution as it can potentially damage the object being imaged, particularly in microscopy, in which the light has to be focused onto a very small area. The optical image amplification made possible by the serialization of the 2D image overcomes this problem.

The image amplifier in our STEAM camera is different from 'image intensifiers'. In STEAM, amplification occurs in the optical domain, whereas in image intensifiers, it occurs in the electronic domain. Image intensifiers are complex devices and have a low image-acquisition rate of up to ~10 kHz in continuous mode[24,25], which is adequate for their intended use in night-vision cameras because these only need to operate at the video rate. The limited frame rate is due to the fundamental compromise between gain and bandwidth in all electronic systems, including the image intensifier.

Operation of the STEAM camera is illustrated in Fig. 2c. The figure shows the image of a 2D object captured in the time domain using a real-time oscilloscope. The reconstruction of the 2D spatial image from a one-dimensional (1D) temporal data stream involves the trivial task of simply sorting the 1D vector into a 2D matrix and is described further in Methods. The results clearly demonstrate a modality for optical imaging that is amenable to high-speed operation. The 2D frame corresponds to the envelope of the temporal pulse shown in Fig. 2a. Frames are repeated at intervals of 163 ns (Fig. 2d)—a value that corresponds to a frame rate of 6.1 MHz, which is a record for continuous real-time imaging. The shutter speed is 440 ps (Methods), which is also a record for continuous real-time imaging. For comparison, Fig. 2c shows the image of the same object using a high-sensitivity infrared camera which has a frame rate of 50 Hz, about 120,000 times less than that of the STEAM camera. In this experiment, the 2D dispersed light traverses the object and the image is captured on the camera in its position behind the object.

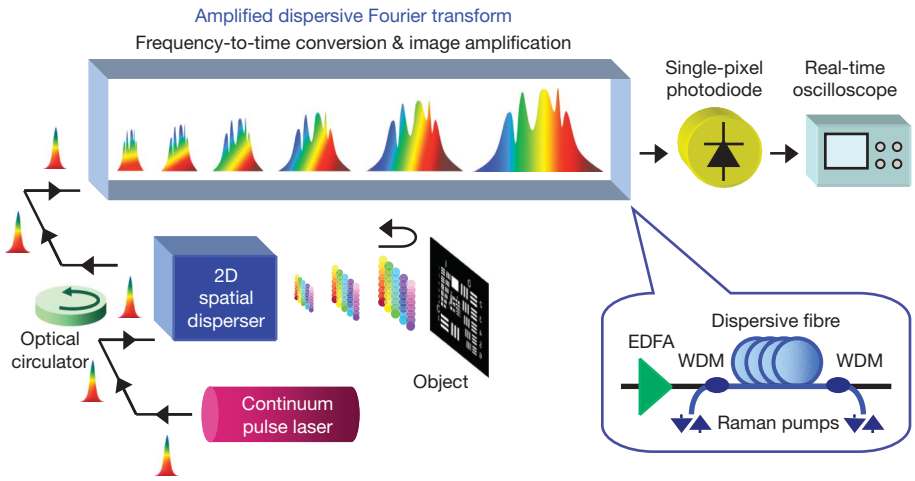

Figure 1 | STEAM camera. The STEAM camera maps a 2D spatial image into a serial time-domain waveform. It starts by encoding the 2D image into the spectrum of a broadband (continuum) pulse (Methods). The optical circulator directs the pulse reflected off the object into an optically amplified dispersive Fourier transformer (inset). An erbium-doped fibre amplifier (EDFA) pre-amplifies the image by 10 dB. The image then enters a dispersive fibre, where it is further boosted by 15 dB using a distributed Raman amplifier pumped by multiple powerful lasers through wavelength-division multiplexers (WDMs), and its spectrum is simultaneously mapped into the time domain. The optical spectrum appears as a serial sequence in time, allowing the image to be captured with a single-pixel photodiode and an oscilloscope. This scheme eliminates the need for a CCD and also performs an image amplification of 25 dB in the optical domain. The amplification enables fast real-time imaging of dynamic events. The STEAM camera can also be used as a confocal microscope (see text). Supplementary Movie 1 illustrates the functionality of the STEAM camera.

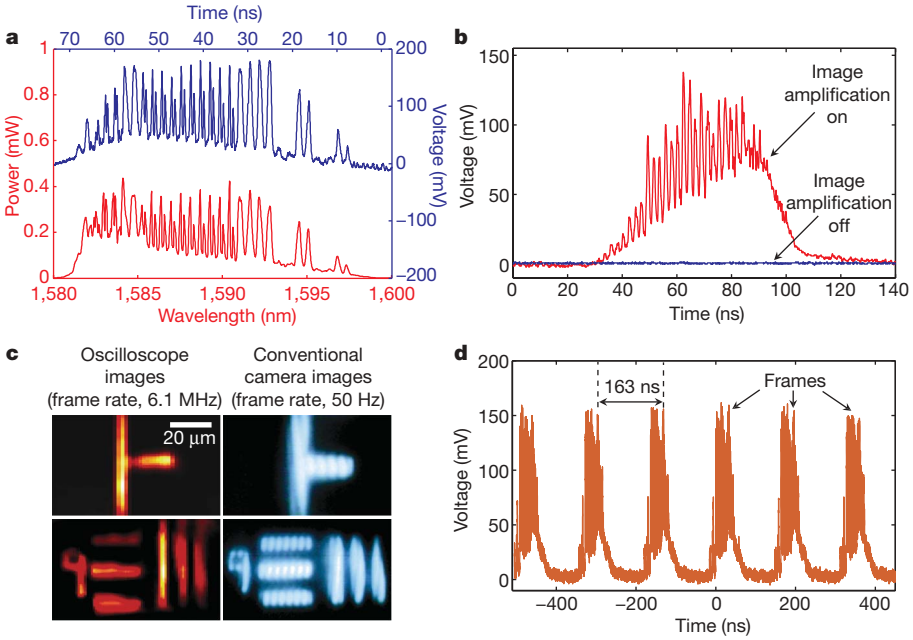

Figure 2 | Basic operation of the STEAM camera. **a**, Comparison between the temporal waveform (single pulse) captured by the oscilloscope (blue) and the spectrum measured by a conventional optical spectrum analyser (red). The consistency between them validates the frequency-to-time mapping operation performed by the dispersive Fourier transformation. **b**, The temporal waveform, representing the image, with (red) and without (blue) the image amplification. The optical amplification raises the otherwise undetectably weak signal significantly above the detector noise floor, overcoming the fundamental compromise between imaging sensitivity and frame rate. **c**, Images of a calibration target captured by the STEAM camera, compared with images obtained using a conventional infrared camera. The shutter speed is estimated to be 440 ps. The granularity in the horizontal direction is an artefact of the particular implementation of the 2D spatial disperser, and is not a fundamental characteristic of the system. **d**, The pulse train captured by the single-pixel photodiode and displayed on the real-time digitizer (oscilloscope). The gap between consecutive pulses is 163 ns. Each pulse contains one frame of the 2D image.

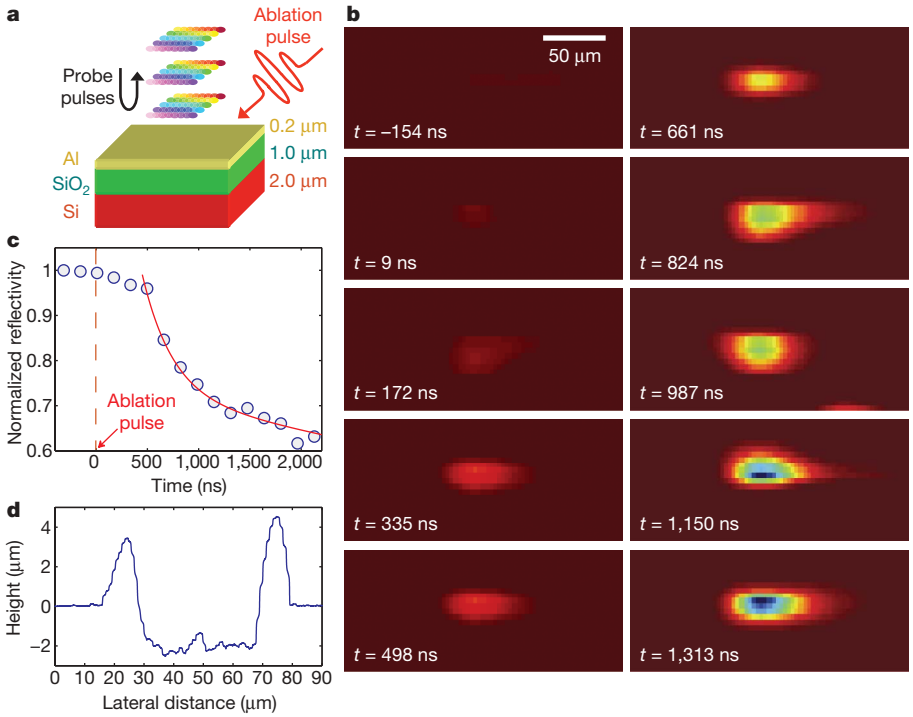

Figure 3 | Schematic of experimental set-up, real-time STEAM images and characterization of the laser ablation experiment. **a**, Schematic set-up for the laser ablation experiment. A mid-infrared pulse laser (6-mJ pulse energy, 5-ns pulse width) is focused at an angle onto the sample with a bilayer of aluminium and silicon dioxide deposited on top of a silicon-on-insulator substrate, while STEAM pulses monitor the ablation process at normal incidence. **b**, Real-time 2D images captured by the STEAM camera with a temporal resolution of 163 ns and shutter speed of 440 ps. The changes in sample surface reflectivity due to the laser-induced mass ejection are evident after the excitation pulse hits the sample at $t = 0$ ns. **c**, The time-sequenced surface reflectivity change showing that the time delay between the pulse excitation and the sudden decrease in the surface reflectivity correlates with the mass-ejection process. This phenomenon is a clear signature of the phase-explosion effect that occurred in the sample. **d**, The depth profile of the sample, obtained with a profilometer, indicating that the ablation pulse ablated the aluminium and silicon dioxide layers and exposed the silicon layer.

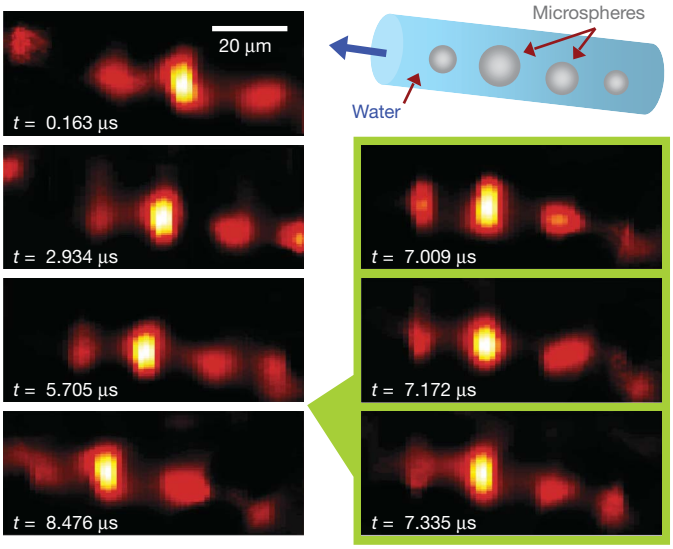

Figure 4 | Schematic and real-time STEAM images of the microfluidics experiment. An ultrafast microfluidic flow of water-suspended metal microspheres (sphere diameters ranging from 10 to 30 μm) was established in a hollow fibre with an inner diameter of 50 μm. On the left, one out of every seventeen snapshots is shown, for clarity. On the right, consecutive snapshots with the full temporal resolution of 163 ns and shutter speed of 440 ps are shown. A total of 3,000 frames can be captured, limited by the memory of the real-time digitizer used in the experiment. A flow of microspheres at a flow speed of about 2.4 m s^{-1} from right to left can be seen. Supplementary Movie 2 is a real-time movie of the microfluidic flow.

As a demonstration of the ultrafast real-time imaging capability of the STEAM camera, we used it to capture the dynamics of laser ablation. Laser ablation is a ubiquitous technology that is used in laser surgery, laser cutting and micromachining, and laser-induced breakdown spectroscopy. The ablation was performed with a mid-infrared pulse laser (with a pulse energy of 6 mJ and a pulse width of 5 ns) focused at an angle onto a sample consisting of a bilayer of aluminium and silicon dioxide deposited on top of a silicon-on-insulator substrate. The imaging pulse train of the STEAM camera was normally incident to the surface of the sample (Fig. 3a). Figure 3b shows the real-time sequence of the images with a frame-repetition period of 163 ns. The entire frame sequence corresponding to the dynamics (laser-induced mass ejection) caused by the single ablation pulse was captured in real time. Further analysis of the surface reflectivity change shows there to be a finite time delay between the pulse excitation and the sudden decrease in the surface reflectivity, which correlates with ejection of material from the sample (Fig. 3c) and is a clear signature of the phase-explosion effect that is the hallmark of laser ablation[18]. Our results also show the depth profile of the sample, and confirm that the laser excitation pulse ablated the aluminium and silicon dioxide layers and exposed the underlying silicon layer. This demonstration firmly establishes the ability of the STEAM camera to monitor fast dynamical processes in real time.

As further proof of the imager's capability, we used the STEAM camera to capture fast microfluidic flow. We set up fast microfluidic laminar flow of water-suspended metal microspheres, with diameters ranging from 10 to 30 μm, in a hollow fibre with a diameter of 50 μm. Figure 4 shows the images captured by the STEAM camera. A total of 3,000 frames were captured in real time, limited only by the memory of the oscilloscope. On the left of the figure, one out of every seventeen snapshots is shown, for clarity; on the right, consecutive frames with the frame resolution of 163 ns are shown. The flow of metal microspheres from the right to the left is clear, and was calculated to have a speed of 2.4 m s^{-1}. A video of the microfluidic flow is available (Supplementary Movie 2). The temporal resolution here is the highest yet achieved in the observation of such ultrafast microfluidic flow. This capability could prove useful in the development of microfluidic biochips, which have the potential to revolutionize cytometry and analysis techniques in molecular biology.

METHODS SUMMARY

The optical source we used was a mode-locked femtosecond laser. The centre wavelength, bandwidth, pulse energy and pulse-repetition rate of the laser after spectral broadening, filtering and pulse picking were 1,590 nm, 15 nm, 82 pJ and 6.1 MHz, respectively. The 2D spectral pattern was produced by the 2D spatial disperser and focused onto the sample using an objective lens. This is an extension of previously demonstrated 1D spectrally encoded imaging[23,26,27], and eliminates the need for mechanical scanning in the second dimension. The 2D disperser comprised a pair of orthogonally oriented dispersers, which consisted of a diffraction grating with a groove density of 1,200 lines per millimetre and a virtually imaged phased array with a free spectral range of 67 GHz and a linewidth of 550 MHz. Such 2D dispersers have previously been used for spectroscopy[20] and wavelength demultiplexing in optical data communications[28].

The amplified dispersive Fourier transformer consisted of a DCF with a total group-velocity dispersion of -3.3 ns nm^{-1}, four ~300-mW continuous-wave pump lasers at 1,470–1,490 nm (chosen to produce a uniform Raman gain profile across the optical fibre bandwidth with ~1-dB variation) and wavelength-division multiplexers that coupled the pump lasers into and out of the DCF. The digitizer had a bandwidth of 16 GHz and a sampling rate of 5×10^{10} samples per second. The captured 1D temporal data was sorted into a 2D matrix in the digital domain for image reconstruction.

The detection sensitivity and minimum detectable reflectivity were -148 dBm Hz^{-1} and 9.2×10^{-7}, respectively. The pixel size and field of view (horizontal × vertical) were found to be 6.4 μm × 0.3 μm and 170 μm × 27 μm, respectively, for Figs 2 and 4, and 16 μm × 0.7 μm and 430 μm × 68 μm, respectively, for Fig. 3.

Full Methods and any associated references are available in the online version of the paper at www.nature.com/nature.

Received 6 December 2008; accepted 2 March 2009.

1. Riehle, R. A. Jr. *Principles of Extracorporeal Shock Wave Lithotripsy* (Churchill Livingstone, 1987).
2. Kodama, R. *et al.* Fast heating of ultrahigh-density plasma as a step towards laser fusion ignition. *Nature* **412,** 798–802 (2001).
3. Epstein, I. R. & Pojman, J. A. *An Introduction to Nonlinear Chemical Dynamics* (Oxford Univ. Press, 1998).
4. Petty, H. R. Spatiotemporal chemical dynamics in living cells: from information trafficking to cell physiology. *Biosystems* **83,** 217–224 (2004).
5. Ohki, K., Chung, S., Ch'ng, Y. H., Kara, P. & Reid, R. C. Functional imaging with cellular resolution reveals precise micro-architecture in visual cortex. *Nature* **433,** 597–603 (2005).
6. Grinvald, A., Frostig, R. D., Siegel, R. M. & Bartfeld, E. High-resolution optical imaging of functional brain architecture in the awake monkey. *Proc. Natl Acad. Sci. USA* **88,** 11559–11563 (1991).
7. Gridley, T. & Woychik, R. Laser surgery for mouse geneticists. *Nature Biotechnol.* **25,** 59–60 (2007).
8. Yanik, M. F. *et al.* Functional regeneration after laser axotomy. *Nature* **432,** 822 (2004).
9. Slade, S. G., Baker, R., Brockman, D. K. & Thornton, S. P. *The Complete Book of Laser Eye Surgery* (Bantam, 2002).
10. Squires, T. M. & Quake, S. R. Microfluidics: fluid physics at the nanoliter scale. *Rev. Mod. Phys.* **77,** 977–1026 (2005).
11. Watson, J. V. *Introduction to Flow Cytometry* (Cambridge Univ. Press, 2004).
12. Huang, B., Wang, W., Bates, M. & Zhuang, X. Three-dimensional super-resolution imaging by stochastic optical reconstruction microscopy. *Science* **319,** 810–813 (2008).
13. Fang, N., Lee, H., Sun, C. & Zhang, X. Sub-diffraction-limited optical imaging with a silver superlens. *Science* **308,** 534–537 (2005).
14. Petty, H. R. Applications of high speed microscopy in biomedical research. *Opt. Photon. News* **15,** 40–45 (2004).
15. Etoh, T. G. *et al.* Evolution of ultra-high-speed CCD imagers. *Plasma Fusion Res.* **2,** S1021 (2007).
16. Barty, A. *et al.* Ultrafast single-shot diffraction imaging of nanoscale dynamics. *Nature Phys.* **2,** 415–419 (2008).
17. Buechler, Ch, Dong, C. Y., So, P. T. C., French, T. & Gratton, E. Time-resolved polarization imaging by pump-probe stimulated emission fluorescence microscopy. *Biophys. J.* **79,** 536–549 (2000).
18. Porneala, C. & Willis, D. A. Observation of nanosecond laser-induced phase explosion in aluminum. *Appl. Phys. Lett.* **89,** 211121 (2006).
19. Solli, D. R., Roper, C., Koonath, P. & Jalali, B. Optical rogue waves. *Nature* **450,** 1054–1057 (2007).

20. Diddams, S. A., Hollberg, L. & Mbele, V. Molecular fingerprinting with the resolved modes of a femtosecond laser frequency comb. *Nature* **445,** 627–630 (2007).
21. Chou, J., Boyraz, O., Solli, D. & Jalali, B. Femtosecond real-time single-shot digitizer. *Appl. Phys. Lett.* **91,** 161105 (2007).
22. Solli, D. R., Chou, J. & Jalali, B. Amplified wavelength-time transformation for real-time spectroscopy. *Nature Photon.* **2,** 48–51 (2008).
23. Goda, K., Tsia, K. K. & Jalali, B. Amplified dispersive Fourier-transform imaging for ultrafast displacement sensing and barcode reading. *Appl. Phys. Lett.* **93,** 131109 (2008).
24. Savage, N. Scientific CCD cameras. *Nature Photon* **1,** 351–353 (2007).
25. Lynch, T. F. & Zeng, A. Image intensified cameras for high-speed imaging applications that require more than just the high frame-rate. *Proc. SPIE* **5580,** 790–795 (2005).
26. Bartelt, H. O. Wavelength multiplexing for information transmission. *Opt. Commun.* **27,** 365–368 (1978).
27. Tearney, G. J., Shishkov, M. & Bouma, B. E. Spectrally encoded miniature endoscopy. *Opt. Lett.* **27,** 412–414 (2002).
28. Xiao, S. & Weiner, A. M. 2-D wavelength demultiplexer with potential for ≥1000 channels in the c-band. *Opt. Express* **12,** 2895–2901 (2004).

Supplementary Information is linked to the online version of the paper at www.nature.com/nature.

Acknowledgements This work was partially supported by the US Defense Advanced Research Projects Agency and the Center for Nanoscience Innovation for Defense. We are grateful to D. R. Solli, Y. Hoshino and T. Kodama for discussions. We also thank T. Lay for creating the animated film.

Author Information Reprints and permissions information is available at www.nature.com/reprints. Correspondence and requests for materials should be addressed to K.G. (goda@ee.ucla.edu).

METHODS

Optical source for the STEAM camera. The optical source used for the STEAM camera was a mode-locked femtosecond laser. A high-nonlinearity fibre was used to generate a supercontinuum with a bandwidth of about 40 nm centred around 1,590 nm. The laser was pulse-picked to reduce the repetition rate to 6.1 MHz using a gated Mach–Zehnder amplitude modulator.

2D spatial disperser. The 2D spatial disperser consisted of a pair of orthogonally oriented spatial dispersers (a virtually imaged phased array (VIPA) and diffraction grating) that produced a 2D spectral pattern which we refer to as a 'spectral shower'. An input pulse is spatially dispersed and separated by the dispersers into many subpulses of different colours. The VIPA was essentially a tilted Fabry–Pérot cavity with a highly reflective coating ($R = 99.9\%$) on one surface except for an uncoated window area and a partially reflective coating ($R \approx 95\%$) on the other surface. A collimated laser beam was focused by a cylindrical lens ($f = 200$ mm) onto the highly reflective surface of the VIPA at a small angle ($\sim 3^\circ$) with respect to the propagation direction through the uncoated window area. The multiple interference that occurred inside the VIPA resulted in angular dispersion that is over an order of magnitude larger than that of typical diffraction gratings. The VIPA with a free spectral range (FSR) of 67 GHz and a linewidth of 550 MHz dispersed the spectrum of the pulse in one direction. Wavelengths that differed by integer multiples of the FSR were spatially overlapped with each other. An orthogonally placed diffraction grating with a groove density of 1,200 lines per millimetre was used to separate this degeneracy in the other direction. It resulted in the spectrum of the incident pulse being mapped into a 2D spectral pattern in space, resembling a spectral shower.

Amplified dispersive Fourier transform. Before the amplified dispersive Fourier transformation was performed, the spectrum of the back-reflected spectral shower was pre-amplified using an L-band EDFA and filtered using a band-pass filter centred at 1,590 nm with a pass band of 15 nm. The Raman-amplified dispersive element consisted of (1) a DCF with a total group-velocity dispersion of -3.3 ns nm^{-1}, (2) four $\sim$300-mW continuous-wave pump lasers, positioned at regular length intervals along the DCF, with respective wavelengths of 1,470 nm, 1,480 nm, 1,490 nm and 1,480 nm, and (3) wavelength-division multiplexers that coupled the pump lasers into and out of the DCF. These pump wavelengths were chosen to produce a uniform Raman gain profile across the optical filter bandwidth with $\sim$1-dB variation. The amplified 1D temporal data stream was captured by a single-pixel photodetector with a 10-GHz bandwidth (Discovery Semiconductors) and digitized using a high-speed digital oscilloscope with a 16-GHz bandwidth and a sampling rate of 5×10^{10} samples per second (Tektronix).

Digital image processing. The purpose of the digital image processing was to sort the 1D temporal data stream into a 2D matrix for image reconstruction. This sorting step was done with knowledge of the FSR of the VIPA, which corresponds to the column length of the final image. The dispersion slope of the DCF (which results in nonlinear frequency-to-time mapping) was also included in this step to avoid the skewing problem in the image reconstruction. In addition, the captured waveform was first digitally band-pass-filtered to remove high-frequency noise, and was normalized by the filtered background waveform corresponding to the background image. The resultant image quality was further enhanced by noise removal using the Wiener filter, image interpolation and contrast equalization.

System parameters of the STEAM camera. The field of view, pixel size, detection sensitivity and shutter speed of the STEAM camera were calculated using the experimental parameters. See the Supplementary Information for a complete description of the equations that characterize the following system parameters.

(1) Pixel size and field-of-view. On the basis of the tilt angle and FSR of the VIPA, the diffraction angle ($\sim 65^\circ$) and groove density of the diffraction grating, the centre wavelength and repetition rate of the spectral shower, and the focal length of the objective lens ($\sim$2 mm for imaging the calibration target and microfluidic flow, respectively (Figs 2 and 4), and $\sim$5 mm for imaging the laser ablation (Fig. 3)), the pixel size and field of view (horizontal $\times$ vertical) were found to be 6.4 μm $\times$ 0.3 μm and 170 μm $\times$ 27 μm, respectively, for Figs 2 and 4, and 16 μm $\times$ 0.7 μm and 430 μm $\times$ 68 μm, respectively, for Fig. 3. From these values, the number of pixels was found to be about 2,500 for all the experiments performed in this paper, and can be increased by a few orders of magnitude by increasing the optical bandwidth, the amount of temporal dispersion used in the dispersive Fourier transform process and the sampling rate of the digitizer. In addition, with the aid of virtual time gating and a parallel architecture, the number of pixels per frame can be increased without sacrificing the frame rate (Supplementary Information).

(2) Detection sensitivity. On the basis of the total noise figure (5.6 dB) and the net image gain (25 dB) of the EDFA and Raman amplifier, as well as the bandwidth (10 GHz) and noise-equivalent power (1 pW Hz$^{-1/2}$) of the photodetector, the input referred noise was found to be -148 dBm Hz^{-1}. Furthermore, on the basis of the average power of each pulse incident on the object for the pulse duration, the minimum detectable reflectivity was found to be 9.2×10^{-7}, corresponding to a detection sensitivity (the inverse of the reflectivity) as high as 60 dB.

(3) Shutter speed. The shutter speed was found to be about 440 ps, on the basis of the pulse width of each subpulse of the spectral shower. This can be obtained from the bandwidth of each subpulse (719 MHz), assuming that the pulses are nearly transform-limited and taking dispersion in the optics into consideration.

Laser ablation experiment. The excitation pulse laser used in the laser ablation experiment was an optical parametric oscillator (OPOTEK) pumped by a Nd:YAG Q-switched laser. It generated a high-power pulse with a centre wavelength of 2.8 μm and a pulse width of 5 ns. A lens ($f = 75$ mm) produced a focused pulse with a fluence of about 20 J cm^{-2} at the surface of the sample.

Microfluidics experiment. The microfluidic system used in the microfluidics experiment consisted of a 15-cm-long hollow fibre with an inner diameter of 50 μm. The metal microspheres, which had diameters ranging from 10 to 30 μm (Thermo Fisher Scientific), were suspended in water with a small amount of ethanol (for wetting the microspheres).